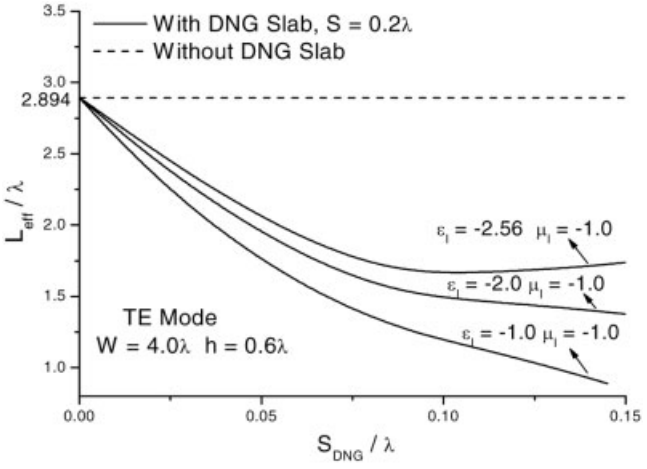

Figure 8 Dependence of the length for a complete power coupling L_{eff} on the thickness of the DNG slab S_{DNG}

cases with DNG slab core, the coupling length is always shorter than that without the DNG slab. Figure 7 shows that the wider separation of the two uniform coupling waveguides, the longer the coupling length is needed to achieve complete power transfer. This is easy to be understood because a wider separation attenuates the amplitude of the evanescent wave penetrating into the uniform coupling waveguides. The complete coupling length becomes larger under higher reflective index of the DNG slab. This is because the electromagnetic field of evanescent wave mainly distributes around the surface of the DNG slab, a DNG slab core with higher reflective index having less electromagnetic field around its surface and thus weakens the evanescent wave penetrating into the uniform coupling waveguides. Similar situation occurs in the case depicted in Figure 8. The surface around which the electromagnetic field mainly distributes approaches the coupling waveguides as the DNG slab core grows thicker, thus more evanescent wave reaches the coupling waveguides and shortens the coupling length for 0-dB coupler.

4. CONCLUSION

In this article, a novel dielectric waveguide directional coupler utilizing a DNG slab core located between the two uniform coupling waveguides is analyzed by a method which combines the building block approach and multimode network theory with a rigorous mode-matching procedure. The scattering and coupling characteristics under different structural and constitutive parameters of the coupler are carefully investigated. Numerical results demonstrate the proposed coupler is more compact and practical by significantly shorten the transition and coupling length.

ACKNOWLEDGMENT

This work is supported by the National Natural Science Foundation of China (No. 60471037 and No. 63531020).

REFERENCES

1. V.G. Veselago, The electrodynamics of substances with simultaneously negative values of ε and μ, Usp Fiz Nauk 92 (1967), 517–526.
2. J.B. Pendry, Negative refraction makes a perfect lens, Phys Rev Lett 85 (2000), 3966–3969.
3. D.K. Qing and Gang Chen, Enhancement of evanescent waves in waveguides using metamaterials of negative permittivity and permeability, Appl Phys Lett 84 (2004).
4. S.T. Peng, Transitions in millimeter waveguides, SPIE Millimeter Wave Technol 544, 71.1085.
5. S.T. Peng and A.A. Oliner, Guidance and leakage properties of a class of the open dielectric waveguides. I. Mathmatical formulation, IEEE Trans MTT MTT-29 (1981), 843–855.
6. Shanjia Xu, S.T. Peng, and F.K. Schwering, Effect of transition waveguides on dielectric waveguide directional couplers, IEEE Trans MTT 37 (1989), 686–690.

© 2007 Wiley Periodicals, Inc.

TEM HORN ANTENNA WITH AN ELLIPTIC PROFILE

J. A. G Malherbe and N. Barnes
Department of Electrical, Electronic and Computer Engineering, University of Pretoria, Pretoria 0002, South Africa

Received 30 November 2006

ABSTRACT: *A variety of profiles for the cross section of wideband TEM horns have been proposed, employing an optimal impedance function or exponential taper in order to minimize reflection losses. In this article, an elliptic longitudinal sectional profile, combined with an optimal impedance function, is proposed and evaluated.* © 2007 Wiley Periodicals, Inc. Microwave Opt Technol Lett 49: 1548–1551, 2007; Published online in Wiley InterScience (www.interscience.wiley.com). DOI 10.1002/mop.22488

Key words: *TEM horn; ultra wideband antenna; elliptic taper*

1. INTRODUCTION

The TEM horn antenna is popular as an ultra-wideband structure, and finds application especially in pulsed systems. Together with modest gain and sidelobe levels, the main consideration for this type of antenna is an excellent input impedance match.

Basic to the design and performance of the TEM horn, is the cross sectional geometry of the transmission line making up the horn. Figure 1 shows a pair of plates of arbitrary shape that constitute a TEM horn. The characteristic impedance of the horn at any given point is determined by the angles α and β that an incremental length of transmission line subtends at the origin. The impedance properties of such a cross section has been extensively treated, most comprehensively in Ref. 1.

The longitudinal section of the horn determines the way in which the field matches in the y-direction. Conventionally, authors have optimized this profile by means of various methods, such as the use of a Hecken near-optimal taper [2–4], exponential taper [5–7], or optimal numerical analysis [8].

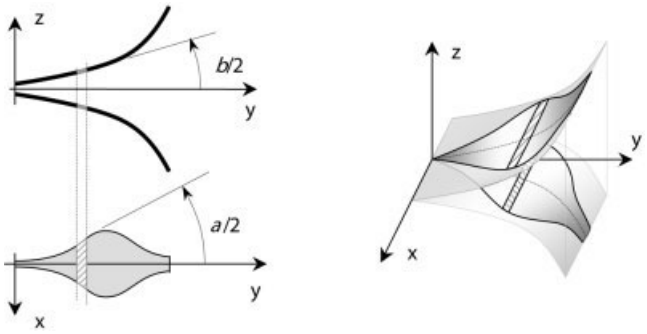

Figure 1 General TEM horn

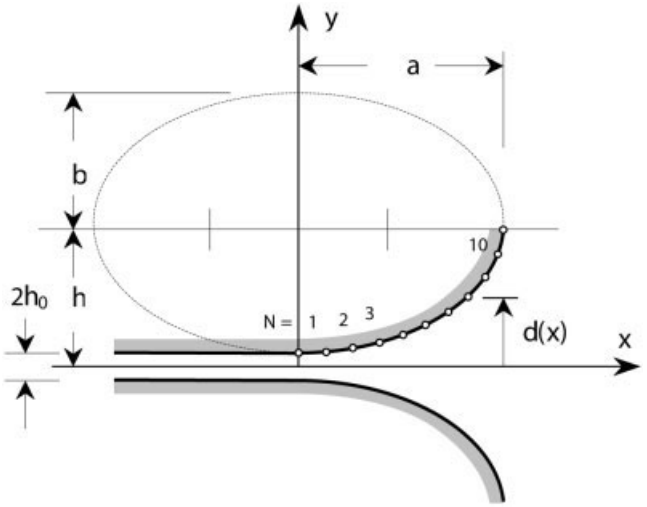

Figure 2 Geometry of elliptic profile

In this article, an elliptic longitudinal sectional profile in the *y–z* plane is chosen, because of its ability to blend the surface smoothly at both the low-impedance (driving point) as well as the free space ends of the horn. The near optimal taper described by Hecken [9] is used to calculate the longitudunal variation of impedance in the horn (along the *y*-axis), and the latter, together with the elliptic profile is then used to obtain the width profile of the horn.

2. DESIGN

2.1. The Elliptic Surface

Two of the prime variables in the design of the elliptic profile horn, are the overall length, a, and the height, $h + h_0$, of the horn: this will determine the horn profile. Referring to Figure 2, the coordinates of the ellipse can be obtained from

$$\frac{x^2}{a^2} + \frac{(y-h)^2}{b^2} = 1, \tag{1}$$

The parameter m is given by

$$m = e^2 = 1 - \frac{b^2}{a^2} \tag{2}$$

where e is the eccentricity of the ellipse. The length of arc described by the ellipse is given by $E(m)$, the complete elliptic integral of the first kind,

$$E(m) = E\left(\frac{1}{2}\pi|m\right) = \int_0^{\pi/2} \sqrt{1 - m\,\sin^2\theta}\,d\theta \tag{3}$$

The arc length is now divided in a number of sections N of equal length along the curvature of the horn (in this case 10), and the coordinates of each section obtained from the incomplete elliptic integral

$$E(\varphi|m) = \int_0^{\varphi} \sqrt{1 - m\,\sin^2\theta}\,d\theta \tag{4}$$

Values for $E(m)$ and $E(\varphi\, m)$ are readily obtained form Ref. 10 (sections 17.1 and 17.6, respectively).

The curved length of the horn directly determines the lowest frequency at which the horn will function. In this case, dimensions of $a = 480$ mm and $b = 366$ mm were chosen, to give $E(m) = 1.9305$, for a curved plate length of $L = 667.47$ mm. Each section of the curved surface thus has a length of 66.75 mm. The lowest usable frequency of the horn thus lies somewhere between ~225 MHz ($L = \lambda/2$) and 450 MHz ($L = \lambda$). The coordinates that define the plate separation along the curve for the $N + 1 = 11$ points is shown in Table 1 (note that the height of the gap where the antenna is driven, $2h_0$, has not been included).

2.2. The Impedance Taper

The procedure for calculating an impedance taper by the method described by Hecken [9] is well known. The length having been chosen and the intervals determined, an optimal taper with a reflection coefficient of 0.01 was chosen, and the corresponding impedance values calculated. The Hecken taper is a bandpass structure, and for this design, the cutoff frequencies were selected to be 500 MHz and 5 GHz, giving a 10:1 bandwidth ratio. The 500 MHz lies well within the lowest frequency that the structure can support.

The impedances thus obtained, together with the given plate separation at the corresponding point on the elliptic curve, is now translated into dimensions for the plate widths. To this end, the standard microstripline approach [11] was used.

$$\begin{aligned} Z_0 &= 60\,\ln\left(\frac{8h}{w} + \frac{w}{4h}\right), && \left(\frac{w}{h}\right) \le 1 \\ Z_0 &= \frac{120\pi}{w/h + 2.42 - 0.44h/w + (1 - h/w)^6}, && \left(\frac{w}{h}\right) \ge 1 \end{aligned} \tag{5}$$

Bear in mind that these equations are for a microstrip of width w over a ground plane at height h; the parallel plates are at $2h$, and consequently the impedance is doubled.

Table 2 shows the calculated impedances over 10 intervals (11 points) as well as the dimensions that would ensure the desired impedance.

2.3. Construction

After the width profile of the two antenna elements were cut, they were shaped over a wooden elliptic profile to obtain the desired plate separation. At the antenna terminals, plate separation was maintained by means of expanded polystyrene spacers, and plate separation was ensured over the rest of the structure by four nylon pillars, as can be seen in Figure 3.

The antenna is not equipped with a conventional balun. A balanced feed is achieved by connecting the outer conductor of the feeding semirigid coax to the underside of one of the antenna surfaces, at a point where a null in current exists [12]. Figure 4 shows the current distribution on the surface at 1 and 4 GHz; the

TABLE 1 Coordinates for Elliptic Profile

N–1	0	1	2	3	4	5	6	7	8	9	10
x	0.00	66.5	132.2	196.6	258.2	316.1	368.7	413.7	449.3	472.0	480.0
y	0.00	3.53	14.1	32.1	57.5	108.6	131.7	180.4	237.1	299.5	365.7

TABLE 2 Impedance and Line Dimensions for Taper

N–1	0	1	2	3	4	5	6	7	8	9	10
x (mm)	0.0	66.5	132.2	196.6	258.2	316.1	368.7	413.7	449.3	472.0	480.0
$Z_0(x)$ (Ω)	50.0	51.5	56.8	69.5	94.4	137.3	199.7	271.4	331.7	365.3	377.0
$d(x)$ (mm)	2.0	9.1	30.3	66.2	116.9	183.2	265.4	362.8	476.3	600.9	733.4
$w(x)$ (mm)	12.1	52.9	156.8	266.2	313.4	285.3	215.4	154.6	121.0	114.4	127.2

nulls can clearly be seen. The semirigid coax is connected to the antenna terminals as shown, thus achieving an excellent balanced feed.

3. MEASUREMENTS

Calculated and measured values of VSWR versus frequency are shown in Figure 5. The measured VSWR stays below 2.0 between 500 MHz and 7.5 GHz (15:1 bandwidth) and below 2.5 from ~250 MHz to 8.2 GHz (30:1).

Calculated and measured responses of gain versus frequency are shown in Figure 6. As the design bandwidth was from 0.5 to 5 GHz, calculated values were only obtained to 5 GHz. However, measurements were done to 10 GHz.

The *E*- and *H*-plane radiation patterns, both calculated and measured, were similarly obtained within the design bandwidth, and are shown in Figures 7 (a) and 7(b) and 8 (a) and 8(b), respectively. In view of the observed increased bandwidth for impedance match and gain, further radiation patterns were measured to 10 GHz, and are also included in Figures 7 and 8. It is of particular importance to note the symmetry of the radiation patterns.

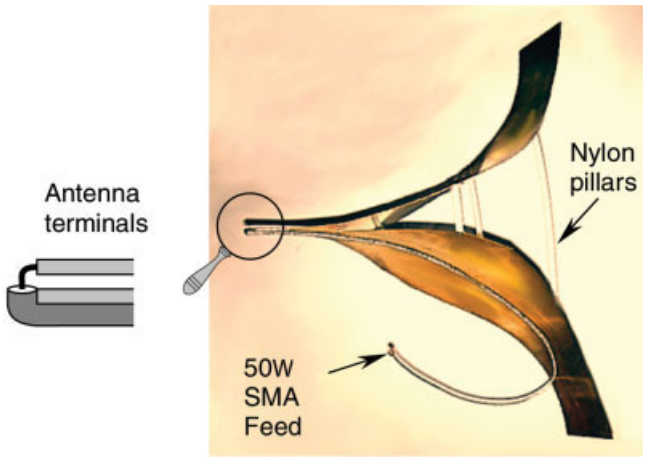

Figure 3 TEM horn, showing attachment of semirigid coax feed. [Color figure can be viewed in the online issue, which is available at www.interscience.wiley.com]

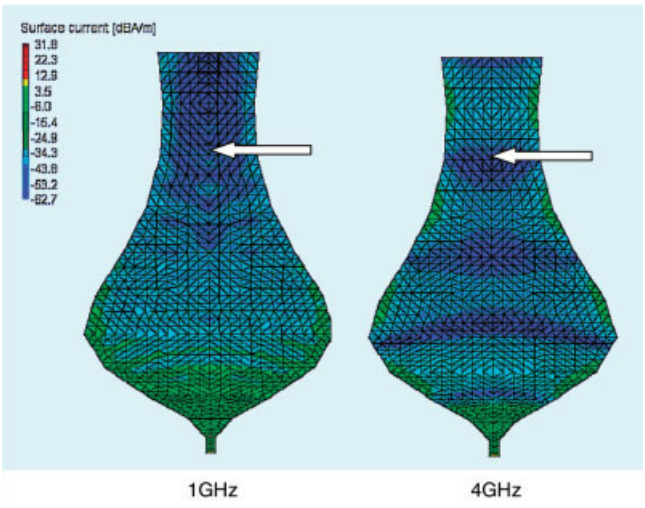

Figure 4 Plots of current distribution at 1 and 4 GHz, showing the null point where the semirigid coax is connected. [Color figure can be viewed in the online issue, which is available at www.interscience.wiley.com]

4. CONCLUSION

The design of an ultra wideband TEM horn antenna with an elliptic profile has been described. It is clear that the elliptic shape leads to a design with extremely low reflection from the aperture of the

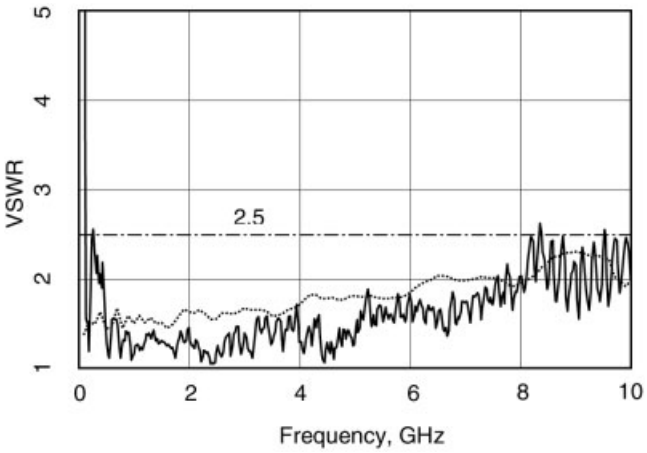

Figure 5 VSWR versus frequency (GHz). Calculated ····· measured——

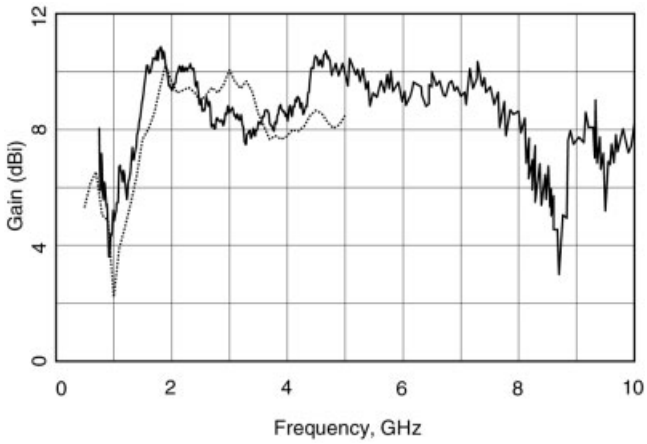

Figure 6 Gain versus frequency (GHz). Calculated ····· measured——

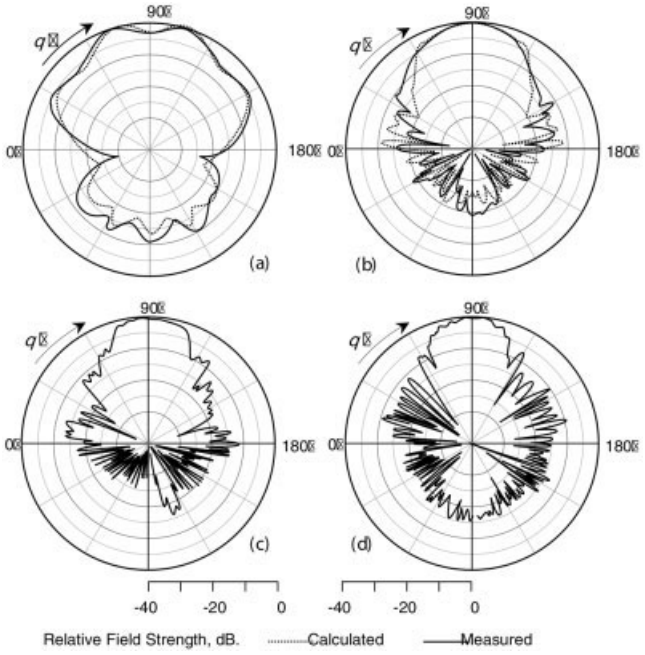

Figure 7 *E*-Plane radiation patterns. (a) 1 GHz, (b) 4 GHz,(c) 8 GHz, and (d) 10 GHz

horn, which was constructed as designed, with no attempt at tuning or improving the impedance performance.

While the band-limited design is for an upper frequency of 5 GHz, it is seen that the horn functions well beyond that frequency. This is because the design is based on the assumption that a true TEM mode exists over the whole of the frequency band. This is, of course, not the case, as the horn radiates a traveling wave as the energy exits the structure; this effect will become all the more pronounced as the frequency increases.

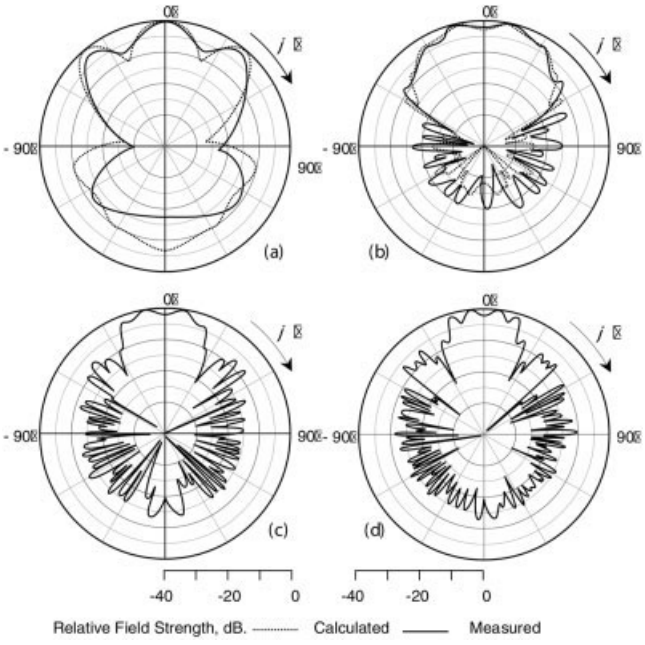

Figure 8 *H*-Plane radiation patterns. (a) 1 GHz, (b) 4 GHz, (c) 8 GHz, and (d) 10 GHz

With minimal effort, a substantial increase in bandwidth can be obtained, if the structure is built with more care. The symmetry of the radiation patterns is an indication of the excellent balance in the feed.

REFERENCES

1. R.T. Lee and G.S. Smith, On the characteristic impedance of the TEM horn antenna, IEEE Trans AP, 52 (2004), 315–318.
2. E.A Theodoruo, M.R. Gorman, P.R. Rigg, and F.N. Kong, Broadband pulse-optimised antenna, IEE Proc H 3 (1981), 124–130.
3. Y. Huang, M. Nakhkash, and J.T. Zhang, A dielectric material loaded TEM horn antenna, ICAP 2003, 12th Intl Conf Ant Prop, ICAP 2003, Vol. 2, 31 March–3 April 2003, pp. 489–492.
4. K.L. Shlager, G.S. Smith, and J.G. Maloney, Accurate analysis of TEM horn antennas for pulse radiation, IEEE Trans Electromagn Compat 38 (1996), 414–423.
5. D.A. Kolokotronis, Y. Huang, and J.T. Zhang, Design of TEM horn antennas for impulse radar, High Frequency Postgrad Stud Colloq 17 (1999), 120–126.
6. H. Choi and S Lee, Design of an exponentially-tapered TEM horn antenna for the wide broadband communication, Microwave Opt Technol Lett 40, (2004) 531–534.
7. K. Chung, S. Pyun, and J. Choi, Design of an ultrawide-band TEM horn antenna with a microstrip-type balun, IEEE Trans Antennas Propagat 53 (2005) 3410–3413.
8. A.S. Turk, Ultra-wideband TEM horn design for ground penetrating impulse radar systems, Microwave Opt Technol Lett 41 (2004) 333–336.
9. R.P Hecken, A near-optimum matching section without discontinuities, IEEE Microwave Theory Tech 20 (1972), 734–739.
10. M. Abramowitz and I.A. Stegun (Eds.), Handbook of mathematical functions, Dover, New York, 1972.
11. R.F.S. Ross and M.J. Howes, Simple formulas for microstrip lines, Electron Lett, 12 (1976), 410.
12. M. Manteghi and Y. Rahmat-Samii, A novel UWB feeding mechanism for the TEM horn antenna, reflector IRA, and the Vivaldi antenna, IEEE Antennas Propagat Mag 46 (2004), 81–87.

© 2007 Wiley Periodicals, Inc.

OPTICAL PROPERTIES OF SIC/SiO_2 COMPOSITE THIN FILM

Jian Yi, XiaoDong He, Yue Sun, and Yao Li
Center for Composite Materials, Harbin Institute of Technology, P.O. Box 3010, Harbin 150001, China

Received 1 December 2006

ABSTRACT: *SiC film was deposited by electron beam-physical vapor deposition on thermal oxidized silicon substrates at 750°C, and SiC/SiO_2 composite thin film was prepared. The obtained composite film was analyzed by Fourier-transform infrared (FTIR) transmission and reflection spectroscopy, and the film reveals an amorphous structure and a high emissivity.* © 2007 Wiley Periodicals, Inc. Microwave Opt Technol Lett 49: 1551–1553, 2007; Published online in Wiley InterScience (www.interscience.wiley.com). DOI 10.1002/mop.22487

Key words: *optical; SiC; SiO_2; FTIR; EB-PVD*

1. INTRODUCTION

SiC is a promising multifunctional protective coating material for metal thermal protection systems because of their combination of unique physicochemical and mechanical properties in rigid condition, such as ultra high velocity and temperature condition [1, 2].